Bioorganic & Medicinal Chemistry 20 (2012) 3223–3232

Contents lists available at SciVerse ScienceDirect

Bioorganic & Medicinal Chemistry

journal homepage: www.elsevier.com/locate/bmc

COMPARE analysis of the toxicity of an iminoquinone derivative of the imidazo[5,4-*f*]benzimidazoles with NAD(P)H:quinone oxidoreductase 1 (NQO1) activity and computational docking of quinones as NQO1 substrates

Vincent Fagan [a], Sarah Bonham [a], Michael P. Carty [b], Patricia Saenz-Méndez [c], Leif A. Eriksson [d], Fawaz Aldabbagh [a,*]

[a] School of Chemistry, National University of Ireland Galway, University Road, Galway, Ireland
[b] Centre of Chromosome Biology, Biochemistry, School of Natural Sciences, National University of Ireland Galway, University Road, Galway, Ireland
[c] Computational Chemistry and Biology Group, Facultad de Química, UdelaR, Montevideo 11800, Uruguay
[d] Department of Chemistry and Molecular Biology, University of Gothenburg, Göteborg 412 96, Sweden

ARTICLE INFO

Article history:
Received 26 February 2012
Revised 26 March 2012
Accepted 26 March 2012
Available online 3 April 2012

Keywords:
Anti-tumor
Bioreductive
DT-diaphorase
Heterocyclic compound

ABSTRACT

Synthesis and cytotoxicity of imidazo[5,4-*f*]benzimidazolequinones and iminoquinone derivatives is described, enabling structure–activity relationships to be obtained. The most promising compound (an iminoquinone derivative) has undergone National Cancer Institute (NCI) 60 cell line (single and five dose) screening, and using the NCI COMPARE program, has shown correlation to NQO1 activity and to other NQO1 substrates. Common structural features suggest that the iminoquinone moiety is significant with regard to NQO1 specificity. Computational docking into the active site of NQO1 was performed, and the first comprehensive mitomycin C (MMC)-NQO1 docking study is presented. Small distances for hydride reduction and high binding affinities are characteristic of MMC and of iminoquinones showing correlations with NQO1 via COMPARE analysis. Docking also indicated that the presence of a substituent capable of hydrogen bonding to the His194 residue is important in influencing the orientation of the substrate in the NQO1 active site, leading to more efficient reduction.

1. Introduction

NAD(P)H:quinone oxidoreductase 1 (NQO1 and also known as DT-diaphorase) is an enzyme which possesses a flavin prosthetic group, and uses NADH or NADPH coenzymes with equal efficiency.[1,2] NQO1 is responsible for obligatory two-electron reduction of quinones to hydroquinones, as well as the reduction of many other substrates including iminoquinones, nitro and azo-compounds.[3] It is often described as a detoxification enzyme since it can override one-electron reductions that generate damaging oxygen radicals by redox recycling,[4] and has been linked with superoxide scavenging ($O_2^{\cdot-}$).[5] Conversely, NQO1 bioreduction can lead to activation of prodrugs, and can induce a cytotoxic or cytostatic effect. Although NQO1 is expressed in normal tissues, elevated levels are known to occur in many human tumor cell lines.[6–8] The cytotoxicity of well-known anti-tumor agents, mitomycin C (MMC) and EO9, show correlation to the levels of NQO1 in the cell lines used at the National Cancer Institute (NCI-60 tumor cell line panel).[6]

Imidazobenzimidazolequinones exist in two heterocyclic arrangements: imidazo[4,5-*f*]benzimidazolequinones and imidazo[5,4-*f*]benzimidazolequinones. Examples of the former were first reported by Schulz and Skibo. Dipyrrolo ring-fused compound **1a** was shown to be an excellent substrate for rat liver NQO1, with high specificity towards melanoma cell lines (Fig. 1).[9] In a subsequent article, molecular modeling studies showed that dipyrido ring-fused analog **1b** was capable of forming stable substrate complexes with human NQO1.[10] More recently, Fagan et al., reported the synthesis and cytotoxicity evaluation of imidazo[5,4-*f*]benzimidazolequinones, containing alicyclic and [1,4]oxazino fused rings (Fig. 2).[11,12] Cytotoxicity was assessed using two human cancer cell lines reported to possess high NQO1 activity; cervical (HeLa),[7] and prostate (DU-145)[6] cancer cells, and a human normal fibroblast cell line (GM00637).

The dipyridoimidazo[5,4-*f*]benzimidazolequinone **2b** was marginally more potent towards the two human cancer cell lines than its isomeric [4,5-*f*] analog **1b** (Table 1). Iminoquinone **2a** was the most potent imidazobenzimidazole evaluated towards the prostate cancer DU-145 cell line, being about 12 times more toxic towards this cell line than towards the normal cell line.[11] The DU-145 cell line is one of the 60 cell lines in the Developmental Therapeutics Program (DTP) at the National Cancer Institute (NCI).[13] One quinone

* Corresponding author. Tel.: +353 (0) 91 493120; fax: +353 (0) 91 495576.
E-mail address: fawaz.aldabbagh@nuigalway.ie (F. Aldabbagh).

0968-0896/$ - see front matter © 2012 Elsevier Ltd. All rights reserved.
http://dx.doi.org/10.1016/j.bmc.2012.03.063

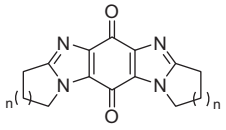

Figure 1. Imidazo[4,5-*f*]benzimidazolequinones.

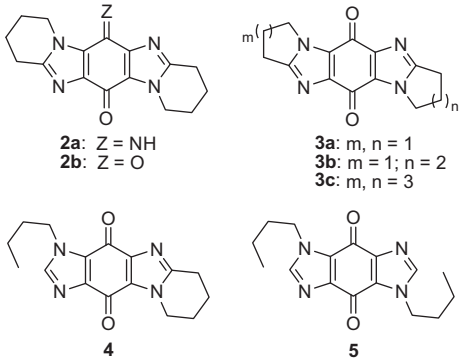

Figure 2. Reported and new imidazo[5,4-*f*]benzimidazolequinones.

and two iminoquinones, including compound **2a**, were submitted for this more detailed in vitro cytotoxicity analysis by the DTP NCI-60 screen, and we now present this data along with the results of COMPARE analysis[13] revealing interesting structure–activity relationships (SARs) with regard to specificity towards NQO1. We also establish SARs for the toxicity of fused alicyclic and nonfused compounds, including the synthesis and evaluation of novel quinones **3a**, **3c**, **4** and **5**. The first comprehensive computational docking study of the clinical drug mitomycin C (MMC) into the human NQO1 active site is provided, along with that of the imidazobenzimidazoles, in order to determine the substrate structural requirements for efficient NQO1 reduction, and to assess the relationship between cytotoxicity and protein–ligand interactions.

2. Results and discussion

2.1. Synthesis

Dipyrrolo- and diazepino-fused quinones **3a** and **3c** were prepared from previously reported dipyrrolo- and diazepino-imidazo[5,4-*f*]benzimidazoles, respectively,[11] according to Scheme 1. Nitro compounds **6** and **7** were isolated in high yields (85% and 92%) by treatment with concentrated nitric and sulfuric acid. Nitro compounds **6** and **7** were catalytically hydrogenated, and Frémy oxidation of the resultant amine intermediates performed under acidic conditions (pH 4), gave mixtures of iminoquinone

Table 1
Cytotoxicity evaluation using the MTT assay:IC_{50} values (μM)[a].

Entry	Compd	Cell Lines		
		GM00637	HeLa CCL-2	DU-145
1	MMC	0.46 ± 0.09	0.27 ± 0.16	0.17 ± 0.02
2	**1b**[11]	>5.0	3.33 ± 0.47	1.73 ± 0.23
3	**2a**[11]	3.63 ± 0.52	1.55 ± 0.35	0.30 ± 0.01
4	**2b**[11]	>5.0	1.67 ± 0.05	1.99 ± 0.39
5	**3b**[12]	1.27 ± 0.05	0.95 ± 0.10	0.79 ± 0.05
6	**3c**	>5.0	1.78 ± 0.19	4.46 ± 0.16
7	**4**	2.12 ± 0.04	1.28 ± 0.05	1.35 ± 0.11
8	**5**	1.05 ± 0.15	0.44 ± 0.04	1.34 ± 0.06

[a] IC_{50} = concentration of compound required for reduction of mean cell viability to 50% of the control value after incubation for 72 h at 37 °C.

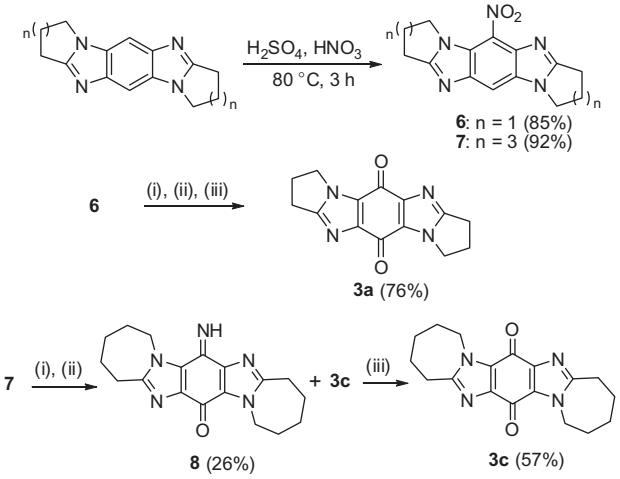

Scheme 1. Synthesis of imidazo[5,4-*f*]benzimidazolequinones **3a** and **3c**. Reagents and conditioins: (i) H_2 (6 bar), Pd-C, MeOH, rt, 16 h; (ii) Frémy's salt (potassium nitrosodisulfonate ($K_2NO(SO_3)_2$)), KH_2PO_4, rt, 1 h; (iii) 2 M HCl, rt, 15 min.

intermediates and their corresponding quinones. Under the same conditions iminoquinone **2a** was isolated in 96% yield from the equivalent Frémy oxidation of the dipyridoimidazo[5,4-*f*]benzimidazole analog.[11] In the case of the dipyrrolo analog, isolation of the iminoquinone proved difficult, thus the mixture was hydrolyzed using HCl (2 M) to give quinone **3a** in 76% yield. The diazepino-fused iminoquinone **8** was separated by chromatography in 26% yield, and the remaining mixture hydrolyzed to give quinone **3c** in 57% yield.

Unsymmetrical imidazo[5,4-*f*]benzimidazolequinone **4**, containing one fused pyrido ring, was accessed according to Scheme 2. Imidazo[5,4-*f*(4,5-*f*)]benzimidazole **9** was alkylated with 1.1 equiv of 1-chlorobutane to give the mono-alkylated compound **10** in 59% yield. Substitution of 1-butyl-5(7)*H*-imidazo[5,4-*f*(4,5-*f*)]benzimidazole **10** with 1-chloro-4-(phenylselenyl)butane gave approximately equal amounts of isomeric phenylselenides **11a** and **11b** in 83% combined yield. Following separation, 1,5-N-disubstituted phenylselenide **11a** was cyclized using a radical substitution protocol.[11] The optimized yield of homolytic aromatic substitution product **12** (87%) was obtained by slow addition of 2.5 equiv of tributyltin hydride (Bu_3SnH) and 2,2′-azobis(cyclohexanecarbonitrile) (ACCN), while exposing the reaction mixture to air for part of the reaction time. The slow addition of the initiator prevents radical reduction by Bu_3SnH, while exposure to air results in oxygenated radicals which are thought to be involved in the final oxidative re-aromatization step (hydrogen atom abstraction).[14,15] The nitration of **12** gave a mixture of nitro isomers which were difficult to separate. Therefore, the mixture was hydrogenated and oxidized to give quinone **4** in 88% yield.

1,5-Dibutylimidazo[5,4-*f*]benzimidazolequinone **5** was prepared in four steps according to Scheme 3. Imidazo[5,4-*f*(4,5-*f*)benzimidazole **9** was dialkylated with 1-chlorobutane (2.2 equiv) giving a separable ~1:1 mixture of 1,5-dibutylimidazo[5,4-*f*]benzimidazole **13a** and 1,7-dibutylimidazo[4,5-*f*]benzimidazole **13b** in 88% overall yield. Nitration of **13a** gave 4-nitroimidazo[5,4-*f*]benzimidazole **14** in 90% yield. This was hydrogenated and oxidized with Frémy's salt to give quinone **5** in 92% yield. No iminoquinone was observed from the synthesis of quinones **4** or **5**.

2.2. Cytotoxicity against normal and cancer cell lines using the MTT assay

The cytotoxicity of new imidazo[5,4-*f*]benzimidazolequinones **3c**, **4** and **5** was evaluated against human cancer cell lines: cervical (HeLa

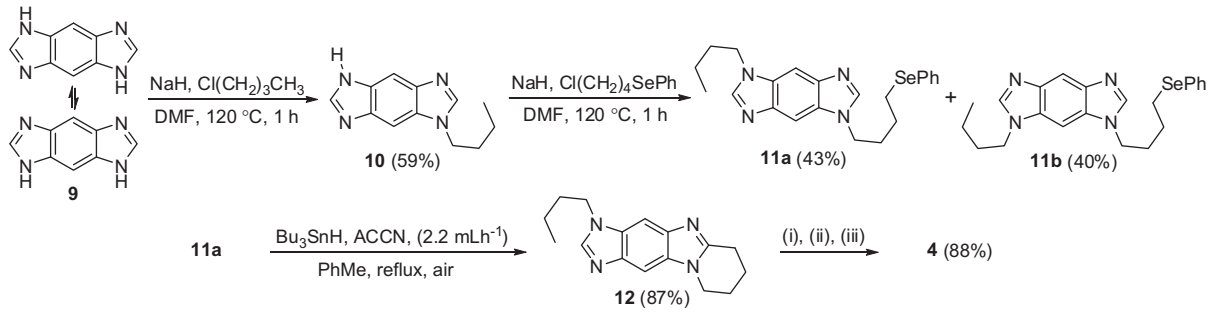

Scheme 2. Synthesis of 3-butylimidazo[5,4-*f*]pyrido[1,2-*a*]benzimidazolquinone **4**. Reagents and conditioins: (i) HNO_3, H_2SO_4, 80 °C, 3 h; (ii) H_2 (6 bar), Pd-C, MeOH, rt, 16 h; (iii) Frémy's salt, KH_2PO_4, rt, 1 h.

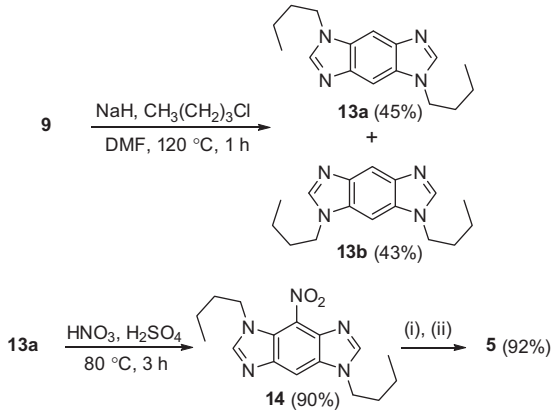

Scheme 3. Synthesis of 1,5-dibutylimidazo[5,4-*f*]benzimidazol-4,8-dione **5**. Reagents and conditioins: (i) H_2 (6 bar), Pd-C, MeOH, rt, 16 h; (ii) Frémy's salt, KH_2PO_4, rt, 1 h.

CCL-2) and prostate (DU-145) cancer. For comparison purposes cytotoxicity against a human normal fibroblast cell line (GM00637) was also determined. Table 1 shows IC_{50} values of **3c**, **4** and **5**, along with that of MMC, and previously reported imidazobenzimidazolequinones evaluated under the same conditions. The cytotoxicity of dipyrroloimidazo[5,4-*f*]benzimidazolequinone **3a** was not obtained due to its poor solubility in organic and aqueous solvents.

The cytotoxicities of pyrrolo–pyrido **3b**, dipyrido **2b** and diazepino **3c** were compared in order to assess the influence that ring size has on the cytotoxicity. Cytotoxicity clearly diminishes as the size of the fused alicyclic ring increases across the series from **3b** to **2b**, to **3c**. Diazepino-fused compound **3c** is about six times less toxic towards the DU-145 cell line than the pyrrolo–pyrido analog **3b**. An increase in cytotoxicity was observed towards all three cell lines, when the extent of ring fusion was decreased from the fully fused system **2b**, to mono-fused pyrido compound **4**, to the nonfused compound **5** (containing no fused pyrido rings). Nevertheless, MMC is the most toxic compound evaluated against all three cell lines. The high potency of MMC may be attributed to the fact that it possesses DNA alkylating functionalities that allow it to form DNA-crosslinks, which induces apoptosis.[16]

2.3. Developmental Therapeutic Program (DTP) National Cancer Institute (NCI) 60 human tumor cell line screen and COMPARE analysis

Iminoquinone **2a** was the most potent imidazobenzimidazole evaluated towards the DU-145 cell line (Table 1), a cell line which is also part of the DTP NCI-60 human tumor cell line screen. Therefore, iminoquinone **2a**, quinone analog **2b**, and diazepino-fused iminoquinone **8**, were submitted for this more detailed cytotoxicity evaluation.

The DTP NCI-60 screen is a two-stage process whereby 60 human tumor cell lines, representing nine major histological tissue types, are initially treated with a single dose of 10 μM of the test compound.[13] The output of the single dose is reported as a mean growth % graph, and a summary is presented in Figure 3 (the full single dose mean growth % graph for each compound is given in the Supplementary data accompanying this article).

In agreement with the MTT assay evaluations (Table 1), iminoquinone **2a** displayed high activity towards the DU-145 cell line, with activity towards melanoma and CNS cancers also observed. Quinone **2b** is inactive using the NCI screen. Increasing the size of the fused alicyclic rings from pyrido to azepino resulted in a loss in activity for iminoquinone **8**, a trend also observed in the MTT assays results for the analogous quinone series.

Iminoquinone **2a** gave a variable toxicity profile, and as a result, was selected for assessment at the subsequent stage of five dose testing. From these results the GI_{50} (concentration of compound required to inhibit cell growth by 50%) for compound **2a** was obtained for each cell line, and a summary is presented in Figure 4 (the full five dose screening results for compound **2a** are given in the Supplementary data accompanying this article). While iminoquinone **2a** was highly active towards DU-145, it was almost inactive towards another prostate cancer cell line, PC-3, which correlates with measured high and low NQO1 activity in the DU-145 and PC-3 cell lines, respectively (Fig. 5). NQO1 has been identified as a molecular target, and its activity in the NCI-60 cell line panel has been quantified.[6] The average NQO1 activity for each cancer type is shown in Figure 5. When Figures 4 and 5 are

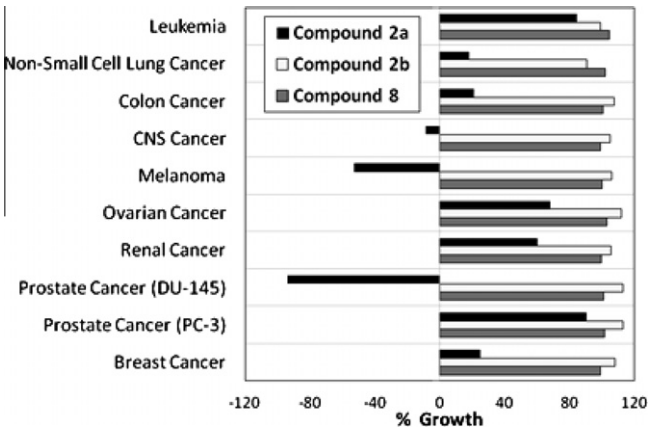

Figure 3. Summary of DTP NCI-60 single dose (10 μM) screening results; reported as the average percent growth of each cancer type (with prostate cancer cell lines shown separately) after treatment with compounds **2a**, **2b** and **8**.

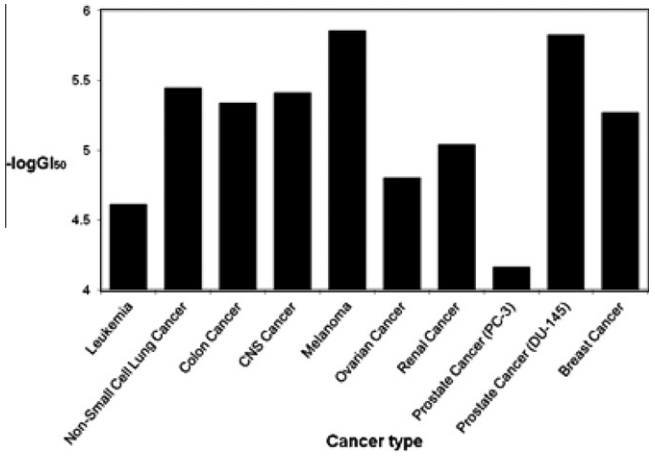

Figure 4. Summary of DTP NCI-60 five dose screening results for iminoquinone **2a**; reported as the average-log GI_{50} on each histological cancer type (with prostate cancer cell lines shown separately). GI_{50} = concentration of compound required to inhibit cell growth by 50%.

compared an overall trend is apparent. Generally, cytotoxicity increases with increased levels of NQO1 activity, and this trend was examined further using the COMPARE software.

The COMPARE program can be accessed through the DTP NCI website (http://dtp.nci.nih.gov/), and can be used to correlate mean graph data with known molecular target levels in the NCI-60 panel (expressed as a pearson correlation coefficient). The data produced can be used to support hypotheses concerning the compound's mechanism of action.[13] COMPARE analysis was performed using the five dose data for **2a**. Compound **2a** showed a moderate to good correlation of 0.51 with NQO1 activity. The clinically used drug MMC is known to be reductively activated by NQO1,[16] and has the highest correlation to NQO1 of the 171 standard agents at the NCI. However, with only a moderate correlation of 0.43, compound **2a** compares favorably (Fig. 6). Compound **2a** was also compared to the ca. 43,000 synthetic compounds in the NCI data base. The two highest correlations were obtained for compounds **15** and **16**, with respective coefficients of 0.87 and 0.77 to iminoquinone **2a**. Compound **15** has a correlation of 0.64 to NQO1, the second highest of all synthetic compounds in the NCI compound database, while compound **16** has a correlation of 0.47 to NQO1. Compounds **15** and **16** possess structural similarities to **2a**, and therefore, it is possible to determine which structural features exert greatest influence on the activity of these molecules. All three molecules have the iminoquinone motif incorporated in some way. All three are flat aromatic molecules with π-stacking capabilities, and all have additional groups or positions with hydrogen bonding capabilities. It seems that the iminoquinone moiety is the most significant structural feature of compound **2a**, and from its correlation to NQO1, and the excellent correlations to other NQO1 substrates, it appears that the iminoquinone moiety is very significant with regard to NQO1 selectivity.

2.4. Computational docking

The NQO1 mechanism of action is described as a ping-pong mechanism, as both NAD(P)H and the quinone substrate must independently occupy the same binding site. NQO1 has a flavin adenine dinucleotide (FAD) redox cofactor that remains bound to the NQO1 protein during the catalytic cycle. The FAD cofactor is reduced to $FADH_2$ by NAD(P)H, and the resulting $NAD(P)^+$ is lost. The quinone substrate now enters the active site and is reduced to a hydroquinone by $FADH_2$. The substrate is then expelled as a hydroquinone, regenerating the NQO1 enzyme (Scheme 4).[1]

Ten compounds were computationally docked into the active site of human NQO1 (PDB code 1D4A).[17,18] The in silico approach allows us to gain insights into the structural requirements for interactions between the quinones and NQO1, and can assist in the design of NQO1 selective compounds. All molecular modeling was performed using the molecular operating environment (MOE) 2009.10 program.[19] The NQO1 crystal structure has two homodimers, each of which is made of two interlocked monomers. The physiological unit of the quinone reductase is a dimer,[20] which was thus employed in the computational modeling. After docking and relaxation/minimization of the structures (for details see Section 4), the interaction energies (I.E.) were calculated (Table 2).

In all cases, the interaction between the ligand and the protein lowers the total energy considerably, leading to stable complexes. The most favorable docking energy was obtained for MMC (−88.4 kcal mol^{-1}). It should, however, be noted that reduction by NQO1 is an activation step and does not directly result in cell death. Therefore the calculated I.E. in Table 2 do not correlate well with the observed cytotoxicity for many of the compounds. Following docking, models of selected ligand–protein complexes were further refined by performing MD simulation and a final energy minimization (rms gradient of 0.01 kcal mol^{-1} $Å^{-1}$) using the LigX

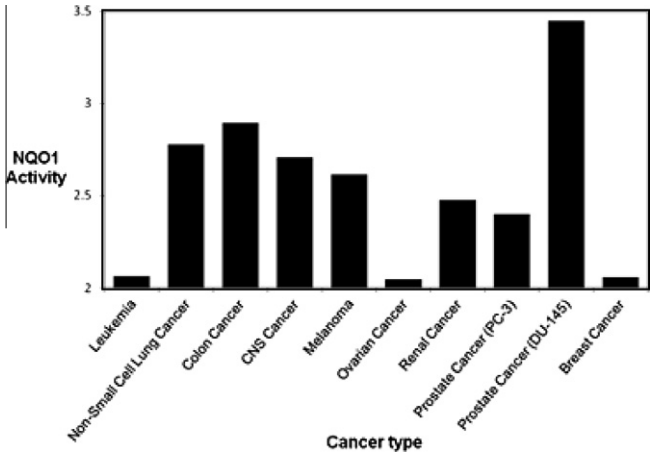

Figure 5. Average NQO1 activity in each of the nine histological cancer types represented in the DTP NCI-60 cell line panel (with prostate cancer cell lines shown separately).

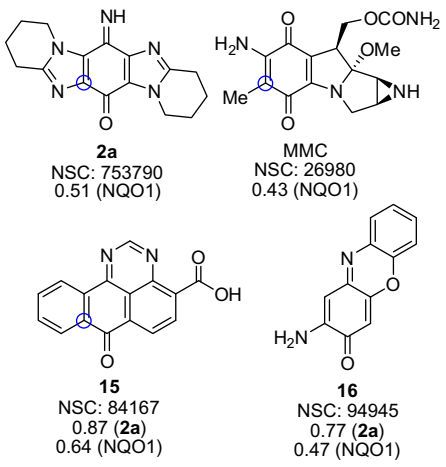

Figure 6. Results of COMPARE analysis of the five dose data for iminoquinone **2a** expressed as pearson correlation coefficients. Blue circle indicates the hydride acceptor carbon in docking studies.

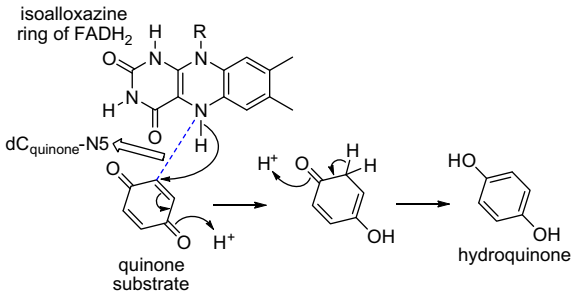

Scheme 4. Transfer of hydride from $FADH_2$ to a quinone in the NQO1 active site; $dC_{quinone}$-N5 indicated by dashed line.

Table 2
Interaction energies of heterocyclic substrates with NQO1

Entry	Complex with NQO1	Interaction energy (I.E.)[a] (kcal mol^{-1})
1	MMC	−88.4
2	**1b**	−63.0
3	**2a**	−64.0
4	**2b**	−76.8
5	**3a**	−53.6
6	**3b**	−56.2
7	**3c**	−61.9
8	**4**	−69.9
9	**5**	−65.1
10	**15**	−59.8

[a] I.E. = $E_{complex}-(E_{enz}+E_{ligand})$.

interface in MOE.[19] In these calculations the protein atoms far from the substrate were constrained not to move, while receptor atoms in the active site, and the quinone substrate in the active site, were treated as flexible. The active site was defined as a distance of 8 Å from the substrate. Several 2D and 3D properties were calculated after energy minimization, including the binding affinity (the estimated binding affinity reported in units of pK_i), and the $C_{quinone}$-N5 distance (Table 3). The binding affinity is that of London ΔG scoring function reported in units of pKi. The affinity ΔG scoring function estimates the contribution to the free energy of binding using a linear function of hydrophobic, ionic, hydrogen bond and metal ligation terms.

For efficient reduction to occur the substrate–protein complex must be stable (i.e., have a high binding affinity), and the substrate must bind in a suitable orientation (i.e., the $C_{quinone}$-N5 distance (Scheme 4) should be within 5 Å) in order to permit the hydride transfer from the reduced $FADH_2$ group to the quinone substrate.

MMC was found to bind with the highest affinity and a short distance to the N5 of the $FADH_2$ isoalloxazine ring, and therefore, is calculated to be efficiently reduced by NQO1. A detailed representation of the MMC-NQO1 active site is shown in Figure 7a. Three residues hydrogen-bond to MMC (namely Gly193, His194 and Tyr126), holding it in a favorable position for reduction to occur. The His194 residue is reported to play an important role in the interaction of quinone substrates with NQO1.[21,22] The oxygen atom of the carbamate (carbonyl) side chain of MMC hydrogen-bonds to His194, influencing the position of MMC in the active site, so that

Table 3
The affinity of selected heterocyclic substrates with NQO1 and the distance between substrate and $FADH_2$ for reduction

Entry	Complex with NQO1	Affinity (units of pKi)	$dC_{quinone}$-N5 (Å)
1	MMC	8.60	3.89
2	**15**	8.53	3.59
3	**2a**	7.41	5.09

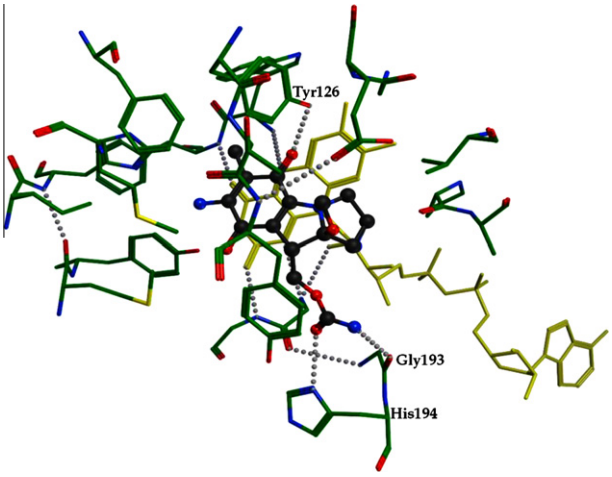

Figure 7a. Molecular model of MMC docked into the active site of NQO1. Hydrogen bonds are shown as dashed lines and the FAD cofactor is shown in yellow.

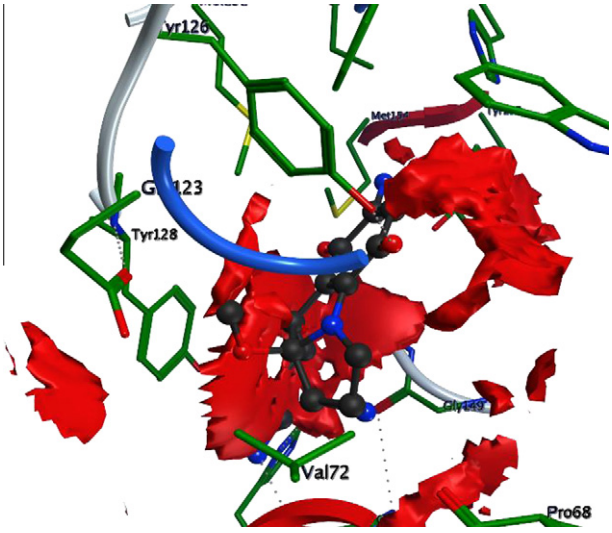

Figure 7b. Hydrophobic contact surface between MMC and NQO1.

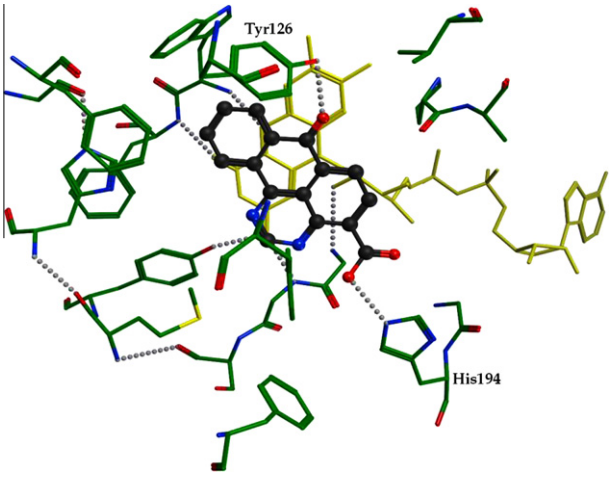

Figure 8a. Molecular model of compound **15** docked into the active site of NQO1. Hydrogen bonds are shown as dashed lines and the FAD cofactor is shown in yellow.

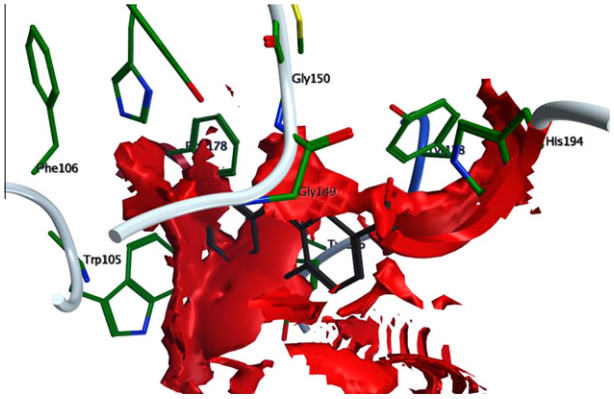

Figure 8b. Hydrophobic contact surface between **15** and NQO1.

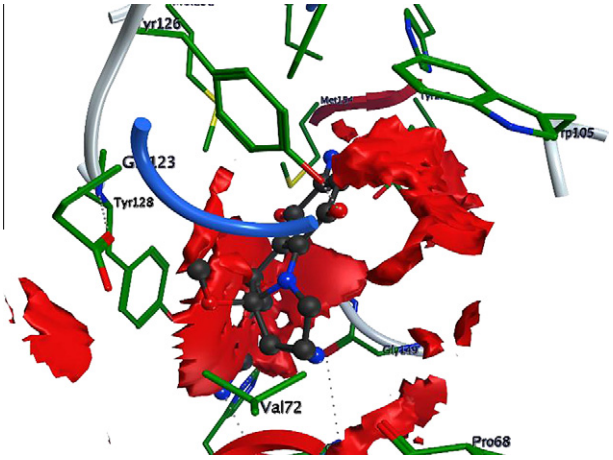

Figure 9b. Hydrophobic contact surface between **2a** and NQO1.

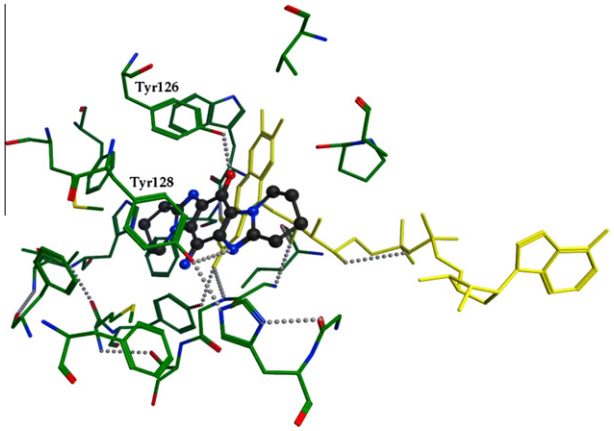

Figure 9a. Molecular model of compound **2a** docked into the active site of NQO1. Hydrogen bonds are shown as dashed lines and the FAD cofactor is shown in yellow.

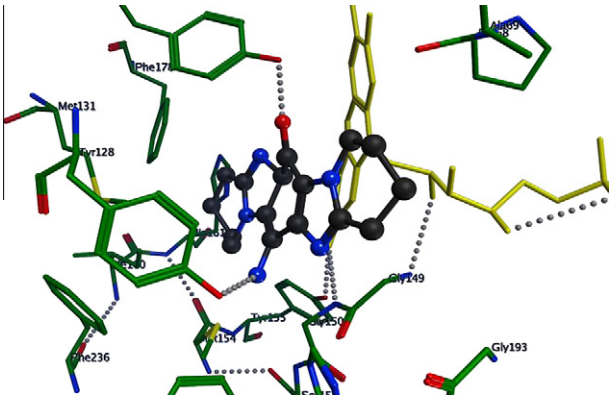

Figure 10. Molecular model of compound **2a** in the active site of NQO1 after hydride transfer. Hydrogen bonds are shown as dashed lines and the FAD cofactor is shown in yellow.

the reactive carbon (indicated in Fig. 6) is located 3.89 Å from the N5 of the $FADH_2$. Further the Trp105 and Tyr128 residues provide a pocket on one side of the active site towards which MMC displays favorable hydrophobic contacts (Fig. 7b).

The docking studies for compound **15** predicted a high affinity and a short $C_{quinone}$-N5 distance (3.59 Å). Hydrogen bonding to Tyr126 and His194, positions the hydride acceptor carbon of compound **15** close to the N5 of the $FADH_2$ group (Fig. 8a). The substrate also shows favorable hydrophobic contacts with Trp105 and Tyr128, as indicated in Figure 8b. However, the calculations show no interactions with the imine nitrogen of the iminoquinone moiety prior to hydride transfer. Interestingly, the His194 forms a hydrogen bond with the carboxyl side chain of **15** in a similar manner to the carbamate group of MMC. This may indicate that the efficiency of NQO1 reduction can be enhanced by the presence of a good hydrogen bonding group (donor or acceptor) located four to five bonds away from the (imino)quinone substructure.

Compound **2a** differs from MMC and compound **15**, in that it lacks a polar group (carbamate or carboxylic acid side chain) and thus, does not hydrogen bond to His194. This may account for its lower affinity and longer $C_{quinone}$-N5 distance. Compound **2a** interacts through hydrogen bonding with Tyr126 and Tyr128 (Fig. 9a), and presents favorable hydrophobic interactions with Pro68, Ala68, Tyr126 and Tyr128 (Fig. 9b). Before reduction, Tyr128 hydrogen bonds to the imidazole nitrogen. Again the calculations show no hydrogen bonding to the imine nitrogen of the iminoquinone of **2a**. After hydride transfer, the phenolic hydroxyl group of Tyr128 rotates to stabilize the resulting negatively charged nitrogen by proton donation (Fig. 10). This model was obtained through energy minimization employing the same force field and definition of the active site (8 Å from the ligand). The charges of the system and the parameters of the reduced ligand were derived employing the semiempirical PM3 hamiltonian. More accurate electronic events resulting from reduction can be evaluated by quantum mechanics methods, but are beyond the scope of this work.

3. Conclusions

Cytotoxicity evaluations have shown that the expansion of the fused alicyclic rings in imidazo[5,4-*f*]benzimidazolequinones and iminoquinones decreases potency, while potency is increased by replacing the fused pyrido rings by *n*-butyl substituents. The DTP NCI-60 cell line screening results of dipyridoiminoquinone **2a** supported the exceptionally high cytotoxicity towards the prostate DU-145 cancer cell line, previously reported using the MTT assay.[11] DTP NCI-60 screening also revealed high potency towards several other tumor cell lines (including some melanoma and CNS cancer cell lines). COMPARE analysis of the DTP NCI-60 screening results for iminoquinone **2a** show a moderate to good correlation of 0.51 to NQO1 activity, and excellent correlations to other synthetic compounds that also show good correlations to NQO1 activity. These compounds share structural similarities, and it seems that the presence of an iminoquinone moiety can increase NQO1

specificity. Computational docking into the NQO1 active site was performed, including the first comprehensive MMC-NQO1 docking study. The binding affinity and $C_{quinone}$-N5 distance were calculated for compounds that showed correlation to NQO1 activity. The presence of a good hydrogen bonding group located four to five bonds away from the (imino)quinone substructure could lead to more efficient NQO1 reduction through interaction with the His194 residue. The absence of such a substituent on compound **2a** may account for its low calculated binding affinity and large $C_{quinone}$-N5 distance. Incorporating such a substituent in future analogs of **2a** may result in greater activity and specificity by increasing the efficiency of reduction by NQO1. The computational docking of iminoquinones showed no extra interactions with NQO1 compared to their quinone counterparts. The greater NQO1 selectivity displayed by the iminoquinones compared to the quinones, may be due to the iminoquinones taking part in fewer competitive biological interactions compared to the quinones. Therefore, the results and conclusions reported here should contribute to the future rational design of more active and selective NQO1 substrates.

4. Experimental section

4.1. General

All materials were obtained commercially, and the synthesis of 2,3,8,9-tetrahydro-1*H*,7*H*-pyrrolo[1,2-*a*]pyrrolo[1′,2′:1,2]imidazo[5,4-*f*]benzimidazole and 2,3,4,5,10,11,12,13-octahydro-1*H*,9*H*-azepino[1,2-*a*]azepino[1′,2′:1,2]imidazo[5,4-*f*]benzimidazole has been reported using a one-pot double radical cyclization protocol.[11] Thin layer chromatography (TLC) was carried out on aluminium-backed plates coated with silica gel (Merck Kieselgel 60 F_{254}). Flash chromatography and dry column vacuum chromatography were carried out using Merck Kieselgel 60H silica gel (particle size 0.040–0.060 mm) and Merck Kieselgel silica gel 60 (particle size 0.015–0.040 mm), respectively, using the specified eluents. Melting points were measured on a Stuart scientific melting point apparatus SMP3. Infrared spectra were recorded using a Perkin–Elmer spec 1 with ATR attached. NMR spectra were recorded using a Joel GXFT 400 MHz instrument equipped with a DEC AXP 300 computer workstation. Chemical shifts are reported in ppm, *J* values are in Hz with Me_4Si as internal standard, and $CDCl_3$ as solvent. All NMR assignments were supported by DEPT and ^1H-^{13}C NMR 2D spectra. High resolution mass spectroscopy was carried out using electrospray ionization (ESI) on a Waters LCT Premier XE spectrometer by manual peak matching. The precision of all accurate mass measurements are better than 5 ppm. Hydrogenation reactions were carried out using a Parr® 5500 series compact reactor.

4.1.1. General procedure for nitration

The imidazo[5,4-*f*]benzimidazole (0.7 mmol) was heated in concentrated H_2SO_4 (10 mL) and concentrated HNO_3 (5 mL) at 80 °C for 3 h. The cooled mixture was diluted with water (100 mL), neutralized with solid Na_2CO_3, and extracted with CH_2Cl_2 (5 × 50 mL). The combined organic extracts were dried (Na_2SO_4), evaporated and the residue purified by dry column vacuum chromatography with gradient elution of EtOAc and MeOH to give the nitro-imidazo[5,4-*f*]benzimidazoles below:

4.1.1.1. 5-Nitro-2,3,8,9-tetrahydro-1*H*,7*H*-pyrrolo[1,2-*a*]pyrrolo[1′,2′:1,2]imidazo[5,4-*f*]benzimidazole (6). 2,3,8,9-Tetrahydro-1*H*,7*H*-pyrrolo[1,2-*a*]pyrrolo[1′,2′:1,2]imidazo[5,4-*f*]benzimidazole gave the 5-nitro imidazo[5,4-*f*]benzimidazole **6** (0.169 g, 85%) as a yellow solid; R_f 0.52 (CH_2Cl_2–MeOH 9:1); mp 245–247 °C; ν_{max} (neat, cm^{-1}) 3225, 1647, 1566, 1522 (NO_2), 1484, 1452, 1409, 1346 (NO_2), 1298, 1271, 1211, 1187, 1117, 1055; δ_H 2.67–2.74 (m, 2H, 2 or 8-CH_2), 2.77–2.85 (m, 2H, 2 or 8-CH_2), 3.11 (t, *J* 7.8, 2H, 3 or 9-CH_2), 3.21 (t, *J* 7.7, 2H, 3 or 9-CH_2), 4.23 (t, *J* 7.1, 2H, 1 or 7-CH_2), 4.54 (t, *J* 7.2, 2H, 1 or 7-CH_2), 7.72 (s, 1H, 11-H); δ_C 23.7, 24.4 (3,9-CH_2), 25.8, 26.1 (2,8-CH_2), 43.6, 48.0 (1,7-CH_2), 106.5 (11-CH), 123.7, 124.8, 129.9, 140.2, 146.5 (all C), 164.1, 165.2 (3a,9a-C); HRMS (ESI): found MH^+, 284.1150. $C_{14}H_{14}N_5O_2$ requires, 284.1147.

4.1.1.2. 7-Nitro-2,3,4,5,10,11,12,13-octahydro-1*H*,9*H*-azepino[1,2-*a*]azepino[1′,2′:1,2]imidazo[5,4-*f*]benzimidazole (7). 2,3,4,5,10,11,12,13-Octahydro-1*H*,9*H*-azepino[1,2-*a*]azepino[1′,2′:1,2]imidazo[5,4-*f*]benzimidazole gave the 7-nitro imidazo[5,4-*f*]benzimidazole **7** (0.219 g, 92%) as a yellow solid; R_f 0.17 (EtOAc–MeOH 9:1); mp 278–280 °C; ν_{max} (neat, cm^{-1}) 3029, 2938, 2923, 2849, 1545, 1520 (NO_2), 1480, 1468, 1442, 1410, 1348 (NO_2), 1305, 1254, 1215, 1190, 1135, 1088, 1045; δ_H 1.74–1.99 (m, 12H), 3.10 (t, *J* 5.3, 2H, 5 or 13-CH_2), 3.16 (t, *J* 5.6, 2H, 5 or 13-CH_2), 4.05–4.15 (m, 2H, 1 or 9-CH_2), 4.19 (t, *J* 4.9, 2H, 1 or 9-CH_2), 7.64 (s, 1H, 15-H); δ_C 25.3, 25.4, 28.1, 28.6, 30.1, 30.4, 30.5, 30.8 (all CH_2), 45.1, 46.8 (1,9-CH_2), 103.2 (15-CH), 124.4, 125.1, 133.2, 133.9, 140.8 (all C), 161.0, 161.1 (5a or 13a-C); HRMS (ESI): found MH^+, 340.1783. $C_{18}H_{22}N_5O_2$ requires, 340.1774.

4.1.2. General procedure for formation of quinones

The nitro-imidazo[5,4-*f*]benzimidazole(s) (0.6 mmol) and Pd-C (5%, 20 mg) were stirred under 6 bar of H_2 in MeOH (100 mL) at room temperature for 16 h. The mixture was filtered, evaporated, and KH_2PO_4 (0.2 M, 100 mL) added. A separate solution of Frémy's salt (0.483 g, 1.8 mmol) in KH_2PO_4 (0.2 M, 50 mL,) was added, and the mixture stirred at room temperature for 1 h. Extracted with CH_2Cl_2 (5 × 50 mL), and evaporated. HCl (2 M, 50 mL) was added to the residue, and the solution stirred for 15 min (not required for quinones **4** and **5**). The acidic solution was neutralized with solid Na_2CO_3 and extracted with CH_2Cl_2 (5 × 50 mL). The combined organic extracts were dried (Na_2SO_4), evaporated, and the residue purified by dry column vacuum chromatography with a gradient elution of EtOAc and MeOH to give the quinones below:

4.1.2.1. 2,3,8,9-Tetrahydro-1*H*,7*H*-pyrrolo[1,2-*a*]pyrrolo[1′,2′:1,2]imidazo[5,4-*f*]benzimidazol-5,11-dione (3a). 5-Nitro-imidazo[5,4-*f*]benzimidazole **6** gave quinone **3a** (0.122 g, 76%), as a yellow solid; R_f 0.55 (CH_2Cl_2–MeOH 9:1); mp >350 °C; ν_{max} (neat, cm^{-1}) 3316, 2990, 2957, 1663 (C=O), 1514, 1485, 1438, 1403, 1356, 1301, 1267, 1225, 1214, 1200, 1179, 1040; δ_H 2.69–2.76 (m, 4H, 2,8-CH_2), 2.96 (t, 4H, *J* 7.6, 3,9-CH_2), 4.29 (t, *J* 7.2, 4H, 1,7-CH_2); δ_C 23.0 (3,9-CH_2); 26.5 (2,8-CH_2), 45.4 (1,7-CH_2), 130.7, 145.9, 160.2 (all C), 171.8 (C=O); HRMS (ESI): found MH^+, 269.1047. $C_{14}H_{13}N_4O_2$ requires, 269.1039.

4.1.2.2. 7-Imino-2,3,4,5,10,11,12,13-octahydro-1*H*,9*H*-azepino[1,2-*a*]azepino[1′,2′:1,2]imidazo[5,4-*f*]benzimidazol-15-one (8) and 2,3,4,5,10,11,12,13-octahydro-1*H*,9*H*-azepino[1,2-*a*]azepino[1′,2′:1,2]imidazo[5,4-*f*]benzimidazol-7,15-dione (3c). 7-Nitroimidazo[5,4-*f*]benzimidazole **7** gave a gave a ~2.3:1 mixture of iminoquinone **8** and quinone **3c**, respectively. The mixture was purified by dry column vacuum chromatography with gradient elution of EtOAc and MeOH to give iminoquinone **8**. The remaining mixture was hydrolyzed with HCl to give quinone **3c**.

Iminoquinone **8** (50 mg, 26%) as a yellow solid; R_f 0.60 (CH_2Cl_2–MeOH 9:1); mp 260–265 °C decomp; ν_{max} (neat, cm^{-1}) 2940, 2918, 2887, 2842, 1650, 1611, 1518, 1495, 1474, 1439, 1412, 1386, 1356, 1349, 1319, 1278, 1261, 1228, 1090, 1073, 1042, 1009; δ_H 1.63–1.90 (m, 12H), 2.91 (t, *J* 5.7, 2H, 5 or 13-CH_2), 2.97 (t, *J* 5.6, 2H, 5 or 13-CH_2), 4.57–4.66 (m, 2H, 1 or 9-CH_2), 4.76–4.88 (m, 2H, 1 or 9-CH_2), 10.69 (s, 1H, NH); δ_C 25.2, 25.3, 28.4, 29.5, 29.6, 31.0 (all

CH_2), 45.9, 46.4 (1,9-CH_2), 126.2, 131.9, 139.4, 156.4, 156.7, 156.9 (all C), 173.0 (C=O); HRMS (ESI): found MH^+, 324.1827. $C_{18}H_{22}N_5O$ requires, 324.1824.

Quinone **3c** (0.111 g, 57%), as a yellow solid; R_f 0.62 (CH_2Cl_2–MeOH 9:1); mp 340–346 °C decomp; ν_{max} (neat, cm^{-1}) 2950, 2919, 2886, 2842, 1654 (C=O), 1523, 1492, 1474, 1437, 1373, 1357, 1346, 1318, 1280, 1241, 1227, 1180, 1093, 1076, 1055, 1016; δ_H 1.69–1.94 (12H, m), 2.99 (4H, t, *J* 5.6, 5,13-CH_2), 4.56–4.64 (4H, m, 1,9-CH_2); δ_C 25.0 (CH_2), 28.2 (CH_2), 29.4 (5,13-CH_2), 30.9 (CH_2), 46.0 (1,9-CH_2), 130.5, 141.4, 157.8 (all C), 172.7 (C=O); HRMS (ESI): found MH^+, 325.1652. $C_{18}H_{21}N_4O_2$ requires, 325.1665.

4.1.3. General procedure for alkylation

Imidazo[5,4-*f*(4,5-*f*)]benzimidazole **9** or **10** (3.2 mmol) and NaH (84 mg, 3.5 mmol) in DMF (50 mL) were heated at 120 °C for 10 min. 1-Chlorobutane (0.322 g, 3.5 mmol for **10** and 0.653 g, 7.1 mmol for **13a** and **13b**) or 1-chloro-4-(phenylselenyl)butane (0.868 g , 3.5 mmol) for **11a** and **11b** was added and the mixture stirred for 1 h. The cooled mixture was evaporated, CH_2Cl_2 added, and filtered. The filtrate was evaporated and the residue purified by dry column vacuum chromatography with gradient elution of EtOAc and MeOH to give the following imidazobenzimidazoles:

4.1.3.1. 1-Butyl-5(7)*H*-imidazo[5,4-*f*(4,5-*f*)]benzimidazole (10). (0.400 g, 59%), as a white solid; R_f 0.18 (EtOAc–MeOH 4:1); mp >350 °C; ν_{max} (neat, cm^{-1}) 3072, 2935, 1577, 1508, 1476, 1446, 1436, 1371, 1284, 1225, 1210, 1136, 1115, 1059, 1021; δ_H 0.94 (t, *J* 7.4, 3H, CH_3), 1.32–1.42 (m, 2H), 1.87–1.94 (m, 2H), 4.21 (t, *J* 7.1, 2H, NCH_2), 7.68 (bs, 1H), 7.92 (bs, 1H), 7.95 (s, 1H), 8.15 (s, 1H), NH not observed; δ_C 13.7 (CH_3), 20.2 (CH_2), 31.6 (CH_2), 45.2 (NCH_2), 131.9 (C), 141.7 (C), 141.9 (CH), 144.1 (CH); HRMS (ESI): found MH^+, 215.1291. $C_{12}H_{15}N_4$ requires, 215.1297.

4.1.3.2. Phenylselenides 11a and 11b. *4.1.3.2.1. 1-Butyl-5-(4-(phenylseleno)butyl)imidazo[5,4-**f**]benzimidazole (**11a**).* (0.586 g, 43%), as a white solid; R_f 0.32 (EtOAc–MeOH 9:1); mp 287–293 °C; ν_{max} (neat, cm^{-1}) 3244, 2956, 1647, 1525, 1490, 1447, 1359, 1287, 1173, 1115, 1082; δ_H 0.94 (t, *J* 7.4, 3H, CH_3), 1.31–1.41 (m, 2H), 1.67–1.75 (m, 2H), 1.86–1.93 (m, 2H), 2.00–2.08 (m, 2H), 2.87 (t, *J* 7.1, 2H, CH_2SePh), 4.17–4.23 (m, 4H, NCH_2), 7.16–7.24 (m, 3H, Ph-H), 7.40–7.44 (m, 2H, Ph-H), 7.72 (s, 1H, 4 or 8-H), 7.74 (s, 1H, 4 or 8-H), 7.88 (s, 1H, 2 or 6-H), 7.95 (s, 1H, 2 or 6-H); δ_C 13.7 (CH_3), 20.1 (CH_2), 27.2 (CH_2SePh), 27.3, 29.4, 31.5 (all CH_2), 44.8, 45.1 (NCH_2), 99.1, 99.2 (4,8-CH), 127.1 (Ph-CH), 129.2 (Ph-CH), 129.8, 131.4, 131.6 (all C), 132.9 (Ph-CH), 141.6 (C), 141.7 (C), 144.1, 144.3 (2,6-CH); HRMS (ESI): found MH^+, 427.1399. $C_{22}H_{27}N_4{}^{80}Se$ requires, 427.1401.

*4.1.3.2.2. 1-Butyl-7-(4-(phenylseleno)butyl)imidazo[4,5-f]benzimidazole (**11b**).* (0.545 g, 40%), as a white solid; R_f 0.11 (EtOAc–MeOH 9:1); mp 78–80 °C; ν_{max} (neat, cm^{-1}) 3374, 3100, 2956, 2930, 2871, 1718, 1683, 1636, 1577, 1524, 1493, 1477, 1456, 1436, 1362, 1263, 1211, 1144, 1112, 1064, 1021; δ_H 0.94 (t, *J* 7.4, 3H, CH_3), 1.30–1.40 (m, 2H), 1.66–1.73 (m, 2H), 1.83–1.90 (m, 2H), 1.99–2.06 (m, 2H), 2.87 (t, *J* 7.0, 2H, CH_2SePh), 4.13–4.23 (m, 4H, NCH_2), 7.15–7.23 (m, 4H, Ph-H & 8-H), 7.34–7.39 (m, 2H, Ph-H), 7.81 (s, 1H, 2 or 6-H), 7.89 (s, 1H, 2 or 6-H), 8.20 (s, 1H, 4-H); δ_C 13.7 (CH_3), 20.1 (CH_2), 27.1 (CH_2), 27.2 (CH_2SePh), 29.1, 31.5 (all CH_2), 44.6 , 45.0 (NCH_2), 88.5 (8-CH), 110.2 (4-CH), 127.1 (Ph-CH), 129.2 (Ph-CH), 129.6, 131.8, 132.0 (all C), 132.8 (Ph-CH), 141.1 (2 × C), 143.5, 143.7 (2,6-CH); HRMS (ESI): found MH^+, 427.1386. $C_{22}H_{27}N_4{}^{80}Se$ requires, 427.1401.

4.1.3.3. Dibutylimidazobenzimidazoles 13a and 13b. *4.1.3.3.1. 1,5-Dibutylimidazo[5,4-f]benzimidazole (**13a**).* (0.389 g, 45%): white solid; R_f 0.42 (EtOAc–MeOH 9:1); mp 209–211 °C; ν_{max} (neat, cm^{-1}) 3093, 3032, 2960, 2930, 2875, 1734, 1516, 1491, 1448, 1370, 1354, 1289, 1223, 1198, 1166, 1117; δ_H (400 MHz, $CDCl_3$) 0.94 (t, *J* 7.4, 6H, CH_3), 1.32–1.41 (m, 4H), 1.87–1.94 (m, 4H), 4.22 (t, *J* 7.1, 4H, NCH_2), 7.73 (s, 2H, 4,8-H), 7.93 (s, 2H, 2,6-H); δ_C (100 MHz, $CDCl_3$) 13.7 (CH_3), 20.1 (CH_2), 31.6 (CH_2), 45.1 (NCH_2), 99.1 (4,8-CH), 131.6 (C), 141.7 (C), 144.3 (2,6-CH); HRMS (ESI): found MH^+, 271.1937. $C_{16}H_{23}N_4$ requires 271.1923.

*4.1.3.3.2. 1,7-Dibutylimidazo[5,4-f]benzimidazole (**13b**).* (0.372 g, 43%): white solid; R_f 0.26 (EtOAc–MeOH 9:1); mp 86–87 °C; ν_{max} (neat, cm^{-1}) 3405, 3226, 3087, 2957, 2930, 2872, 1637, 1525, 1492, 1464, 11450, 1363, 1277, 1262, 1210, 1202, 1137, 1109, 1093, 1010; δ_H (400 MHz, $CDCl_3$) 0.97 (t, *J* 7.4, 6H, CH_3), 1.35–1.44 (m, 4H), 1.87–1.94 (m, 4H), 4.21 (t, *J* 7.1, 4H, NCH_2), 7.21 (s, 1H, 8-H), 7.92 (s, 2H, 2,6-H), 8.19 (s, 1H, 4-H); δ_C (100 MHz, $CDCl_3$) 13.7 (CH_3), 20.2 (CH_2), 31.5 (CH_2), 45.0 (NCH_2), 88.3 (8-CH), 110.4 (4-CH), 132.1 (C), 141.1 (C), 143.7 (2,6-CH); HRMS (ESI): found MH^+, 271.1916. $C_{16}H_{23}N_4$ requires 271.1923.

4.1.4. 3-Butyl-6,7,8,9-tetrahydroimidazo[5,4-*f*]pyrido[1,2-*a*]benzimidazole (12)

To a solution of phenylselenide **11a** (0.600 g, 1.4 mmol) in toluene (50 mL) at reflux under N_2, was added a solution of 1,1'-azobis(cyclohexanecarbonitrile) (ACCN) (0.855 g, 3.5 mmol) and Bu_3SnH (1.019 g, 3.5 mmol) in toluene (50 mL) using a syringe pump at a rate of 2.2 mL h^{-1}. After ~11.5 h the reaction was allowed to proceed in the open air. The cooled mixture was extracted with AcOH (80%, 5 × 20 mL), the combined extracts washed with petroleum ether (3 × 20 mL), and evaporated. Na_2CO_3 solution (5%, 50 mL) was added to the acidic residue, and extracted with CH_2Cl_2 (5 × 50 mL). The combined organic extracts were dried (Na_2SO_4), evaporated, and the residue purified by dry column vacuum chromatography with a gradient elution of EtOAc and MeOH to give imidazobenzimidazole **12** (0.329 g, 87%) as a white solid; R_f 0.33 (EtOAc–MeOH 9:1); mp 238–240 °C; ν_{max} (neat, cm^{-1}) 2924, 2856, 1529, 1477, 1447, 1358, 1314, 1259, 1189, 1119, 1084; δ_H 0.92 (t, *J* 7.4, 3H, CH_3), 1.28–1.38 (m, 2H), 1.84–1.91 (m, 2H), 1.99–2.05 (m, 2H), 2.12–2.18 (m, 2H), 3.10 (t, *J* 6.4, 2H, 6-CH_2), 4.11 (t, *J* 6.1, 2H), 4.20 (t, *J* 7.1, 2H), 7.58 (s, 1H), 7.60 (s, 1H), 7.89 (s, 1H, 2-H); δ_C 13.7 (CH_3), 20.1, 20.9, 22.8 (all CH_2), 25.8 (6-CH_2), 31.6, 42.6, 45.1 (all CH_2), 97.7, 98.3 (4,11-CH), 131.5, 132.5, 140.6, 140.8 (all C), 143.5 (2-CH), 153.1 (5a-C); HRMS (ESI): found MH^+, 269.1759. $C_{16}H_{21}N_4$ requires, 269.1766.

4.1.5. 3-Butyl-6,7,8,9-tetrahydroimidazo[5,4-*f*]pyrido[1,2-*a*]benzimidazol-4,11-dione (4)

A mixture of 4 and 11-nitroimidazo[5,4-*f*]benzimidazoles prepared according to the general procedure for nitration, and subjected to the general procedure for formation of quinones gave quinone **4** (0.157 g, 88%), as a yellow solid; R_f 0.17 (EtOAc–MeOH 9:1); mp 216–217 °C; ν_{max} (neat, cm^{-1}) 3190, 2955, 2871, 1678, 1656 (C=O), 1512, 1488, 1473, 1425, 1377, 1334, 1299, 1266, 1253, 1222, 1193, 1072, 1052; δ_H 0.92 (t, *J* 7.4, 3H, CH_3), 1.29–1.38 (m, 2H), 1.77–1.84 (m, 2H), 1.93–2.07 (m, 4H), 2.96 (t, *J* 6.4, 2H, 6-CH_2), 4.31–4.35 (m, 4H), 7.60 (s, 1H, 2-H); δ_C 13.6 (CH_3), 19.7, 19.8, 22.2 (all CH_2), 25.1 (6-CH_2), 32.4, 45.7, 47.0 (all CH_2), 130.7 (2 × C), 142.2 (C), 142.5 (2-CH), 143.2 (C), 151.6 (C), 171.9 (C=O), 172.1 (C=O); HRMS (ESI): found MH^+, 299.1497. $C_{16}H_{19}N_4O_2$ requires 299.1508.

4.1.6. 1,5-Dibutyl-4-nitroimidazo[5,4-*f*]benzimidazole (14)

Imidazo[5,4-*f*]benzimidazole **13a** was subjected to the general nitration procedure to give **14** (0.199 g, 90%): yellow solid; R_f 0.44 (EtOAc–MeOH 9:1); mp 155–156 °C; ν_{max} (neat, cm^{-1}) 3109, 2949, 2929, 2870, 1763, 1526 (NO_2), 1512, 1498, 1485, 1464, 1436, 1369 (NO_2), 1349, 1333, 1317, 1280, 1230, 1200, 1191,

1125, 1087; δ_H (400 MHz, $CDCl_3$) 0.86 (t, *J* 7.4, 3H, CH_3), 0.93 (t, *J* 7.4, 3H, CH_3), 1.15–1.25 (m, 2H), 1.30–1.39 (m, 2H), 1.58–1.66 (m, 2H), 1.85–1.92 (m, 2H), 4.26 (t, *J* 7.1, 2H, NCH_2), 4.32 (t, *J* 7.2, 2H, NCH_2), 7.97 (s, 1H), 7.99 (s, 1H, 8-H), 8.07 (s, 1H); δ_C (100 MHz, $CDCl_3$) 13.56 (CH_3), 13.58 (CH_3), 19.8, 20.1, 31.7, 32.3 (all CH_2), 45.5 (NCH_2), 47.8 (NCH_2), 105.7 (8-CH), 123.4, 125.9, 131.7, 135.9, 143.7 (all C), 146.4, 147.5 (2 & 6-CH); HRMS (ESI): found MH^+, 316.1769. $C_{16}H_{22}N_5O_2$ requires 316.1774.

4.1.7. 1,5-Dibutylimidazo[5,4-*f*]benzimidazol-4,8-dione (5)

4-Nitro-imidazo[5,4-*f*]benzimidazole **14** was subjected to the general procedure for formation of quinones to give **4** (0.166 g, 92%): yellow solid; R_f 0.44 (EtOAc–MeOH 9:1); mp 213–214 °C; ν_{max} (neat, cm^{-1}) 3068, 2957, 2932, 2871, 1665 (C═O), 1515, 1489, 1459, 1385, 1336, 1217, 1185, 1065, 1033; δ_H (400 MHz, $CDCl_3$) 0.92 (t, *J* 7.4, 6H, CH_3), 1.28–1.37 (m, 4H), 1.78–1.85 (m, 4H), 4.35 (t, *J* 7.2, 4H, NCH_2), 7.64 (s, 2H, 2,6-H); δ_C (100 MHz, $CDCl_3$) 13.6 (CH_3), 19.7 (CH_2), 32.6 (CH_2), 47.1 (NCH_2), 131.0 (C), 142.9 (2,6-CH), 143.5 (C), 172.2 (C═O); HRMS (ESI): found MH^+, 301.1656. $C_{16}H_{21}N_4O_2$ requires 301.1665; elemental analysis Calcd (%) for $C_{16}H_{20}N_4O_2$: C 63.98, H 6.71, N 18.65. Found: C 63.60, H 6.85, N 18.31.

4.2. Cell culture and cytotoxicity evaluation

An SV40-transformed normal human skin fibroblast cell line (repository number GM00637) was obtained from the National Institute for General Medical Sciences (NIGMS) Human Genetic Cell Repository (Coriell Institute for Medical Research, New Jersey, USA). The HeLa cervical cancer cell line (repository number CCL-2) was obtained from the American Type Culture Collection (ATCC). The DU-145 prostate cancer cell line (ATCC repository number HTB-81) was obtained from Professor R.W.G. Watson, School of Medicine & Medical Sciences, University College Dublin, Ireland.

4.2.1. Cell culture

The SV40-transformed normal human skin fibroblast cell line (GM00637) was grown in minimum essential media (MEM) Eagle–Earle BSS supplemented with 15% heat-inactivated fetal bovine serum (FBS), penicillin-streptomycin, 2 mM L-glutamine, 2× essential and nonessential amino acids, and vitamins. HeLa-CCL-2 cervical cancer cells were grown in Dulbecco's Modified Eagle's Medium (DMEM) supplemented with 10% heat-inactivated fetal bovine serum, penicillin–streptomycin, 2 mM L-glutamine, and MEM nonessential amino acids. DU-145 prostate cancer cells were grown in RPMI-1640 medium supplemented with 10% heat-inactivated fetal bovine serum, penicillin–streptomycin and 2 mM L-glutamine.

4.2.2. Cytotoxicity measurement

Cell viability was determined using the MTT colorimetric assay.[23] Normal cells were plated into 96-well plates at a density of 10,000 cells per well (200 μL per well) and allowed to adhere over a period of 24 h. HeLa cells were plated into 96-well plates at a density of 1000 cells per well (100 μL per well) and allowed to adhere over a period of 24 h. DU-145 cells were plated into 96-well plates at a density of 2000 cells per well (200 μL per well) and allowed to adhere over a period of 24 h.

Compound solutions were applied in ethanol (1% final concentration in well), and the plates were incubated at 37 °C under a humidified atmosphere containing 5% CO_2 for 72 h. Control cells were exposed to an equivalent concentration of ethanol alone. MMC (sigma) solutions were applied in DMSO (1% final concentration in well) and the plates were incubated at 37 °C under a humidified atmosphere containing 5% CO_2 for 72 h. Control cells were exposed to an equivalent concentration of DMSO alone. MTT (20 μL, 5 mg/ml solution) was added, and the cells were incubated for another 3 h. The supernatant was removed carefully by pipetting. The resultant MTT formazan crystals were dissolved in 100 μL of DMSO and absorbance was determined on a plate reader at 550 nm with a reference at 690 nm. Cell viability is expressed as a percentage of the EtOH or DMSO-only treated value. Dose-response curves were analyzed by nonlinear regression analysis and IC_{50} values were estimated using GraphPad Prism software, v. 5.02 (GraphPad Inc., San Diego, CA, USA).

4.3. Computational methods

The crystallographic coordinates of human NQO1 (1D4A) were obtained from the RCSB Protein Data Bank. The physiological dimer was used throughout, and hydrogen atoms were added to the protein and the prosthetic group (FAD) based on their protonation state at pH 7. The ligands were built in MOE.

All structures of ligands, enzyme model (NQO1 physiological dimer) and enzyme-ligand complexes were geometry minimized using the AMBER99 molecular mechanics force field[24] to within an rms gradient of 0.05 kcal mol^{-1} $Å^{-1}$. Throughout, all systems were surrounded by a distance dependent dielectric model of bulk water ($E_{SOL} = 0$, $E_{ELECTROSTATIC} = q_i q_j / 4\pi\varepsilon_0 r_{ij}^2$). Where, E_{SOL} represents the implicit solvation energy calculated using the Generalized Born model (GB/VI). To obtain a relaxed geometry of the initial receptor, a short molecular dynamics (MD) simulations was performed, followed by a final energy minimization step. The MD simulation of the NQO1 dimer was performed using a canonical ensemble (NVT), with initial temperature 150 K; heating for 50 ps; simulation temperature 300 K; duration 500 ps; time step 1 fs; temperature response 1 ps; pressure response 0.5 ps and constraint tolerance 1×10^{-9}. After the MD simulation, a final energy minimization was performed. The resulting protein model was used in the docking studies.

Possible active sites in the receptor model were identified by using alpha site finder.[25] Once defined, ligands were docked into the enzyme retaining 500 poses using the alpha triangle placement methodology with affinity ΔG as scoring function as implemented in MOE. In the docking studies, flexible ligand structures were generated using a Monte Carlo algorithm, whereas the receptor was held fixed according to the minimized geometries.

Best scored binding orientations for each ligand were energy minimized, subjected to MD simulation using the same settings as above and finally energy minimized, using in all stages the AMBER99 force field. The potential energy of the final complex was calculated ($E_{complex}$). The ligand was then moved away from the protein, the noninteracting system energy minimized, and the potential energy of the separated moieties calculated ($E_{enz} + E_{ligand}$). Subtracting this from $E_{complex}$ gives the interaction energy (I.E.) reported herein. Several properties were calculated for each best scored complex, using the LigX procedure,[19] such as the affinity, hydrogen bond interactions, van der Waals interactions and π–π interactions.

Acknowledgements

We thank the Irish Research Council for Science Engineering and Technology funded by the National Development Plan for awarding an Embark Scholar Award to Vincent Fagan. We also gratefully acknowledge the financial support from National University of Ireland Galway and Science Foundation Ireland for a Research Frontiers Programme Award (07/RFP/CHEF227). We are grateful to Professor William Watson (School of Medicine & Medical Sciences, University College Dublin, Ireland) for the DU-145 cell line.

Supplementary data

Supplementary data (supplementary data includes ^{1}H and ^{13}C NMR spectra of compounds, HPLC chromatograms, cell viability plots, and full NCI, and COMPARE analysis data) associated with this article can be found, in the online version, at http://dx.doi.org/10.1016/j.bmc.2012.03.063.

References and notes

1. Li, R.; Bianchet, M. A.; Talalay, P.; Amzel, L. M. *Proc. Natl. Acad. Sci. U.S.A.* **1995**, *92*, 8846.
2. Skelly, J. V.; Sanderson, M. R.; Suter, D. A.; Baumann, U.; Read, M. A.; Gregory, D. S. J.; Bennett, M.; Hobbs, S. M.; Neidle, S. *J. Med. Chem.* **1999**, *42*, 4325.
3. Ross, D.; Siegel, D. *Methods Enzymol.* **2004**, *382*, 115.
4. Dinkova-Kostova, A. T.; Talalay, P. *Arch. Biochem. Biophys.* **2010**, *501*, 116.
5. Siegel, D.; Gustafson, D. L.; Dehn, D. L.; Han, J. Y.; Boonchoong, P.; Berliner, L. J.; Ross, D. *Mol. Pharmacol.* **2004**, *65*, 1238.
6. Fitzsimmons, S. A.; Workman, P.; Grever, M.; Paull, K.; Camalier, R.; Lewis, A. D. *J. Natl Cancer Inst.* **1996**, *88*, 259.
7. Bello, R. I.; Gómez-Díaz, C.; Navarro, F.; Alcaín, F. J.; Villalba, J. M. *J. Biol. Chem.* **2001**, *276*, 44379.
8. Kolesar, J. M.; Pritchard, S. C.; Kerr, K. M.; Kim, K.; Nicolson, M. C.; McLeod, H. *Int. J. Oncol.* **2002**, *21*, 1119.
9. Schulz, W. G.; Skibo, E. B. *J. Med. Chem.* **2000**, *43*, 629.
10. Suleman, A.; Skibo, E. B. *J. Med. Chem.* **2002**, *45*, 1211.
11. Fagan, V.; Bonham, S.; Carty, M. P.; Aldabbagh, F. *Org. Biomol. Chem.* **2010**, *8*, 3149.
12. Fagan, V.; Bonham, S.; McArdle, P.; Carty, M. P.; Aldabbagh, F. *Eur. J. Org. Chem.* **2012**, 1967.
13. Shoemaker, R. H. *Nature Rev. Cancer* **2006**, *6*, 813.
14. Bowman, W. R.; Storey, J. M. D. *Chem. Soc. Rev.* **2007**, *36*, 1803.
15. Lynch, M.; Hehir, S.; Kavanagh, P.; Leech, D.; O'Shaughnessy, J.; Carty, M. P.; Aldabbagh, F. *Chem. Eur. J.* **2007**, *13*, 3218.
16. Seow, H. A.; Penketh, P. G.; Baumann, R. P.; Sartorelli, A. C. *Methods Enzymol.* **2004**, *382*, 221.
17. Faig, M.; Bianchet, M. A.; Talalay, P.; Chen, S.; Winski, S.; Ross, D.; Amzel, L. M. *Proc. Natl. Acad. Sci. U.S.A.* **2000**, *97*, 3177.
18. Hassani, M.; Cai, W.; Koelsch, K. H.; Holley, D. C.; Rose, A. S.; Olang, F.; Lineswala, J. P.; Holloway, W. G.; Gerdes, J. M.; Behforouz, M.; Beall, H. D. *J. Med. Chem.* **2008**, *51*, 3104.
19. Molecular Operating Environment, Version 2009.10, Chemical Computing Group: Montreal, QC, 2009.
20. Bianchet, M. A.; Faig, M.; Amzel, L. M. *Methods Enzymol.* **2004**, *382*, 144.
21. Chen, S.; Wu, K.; Zhang, D.; Sherman, M.; Knox, R.; Yang, C. S. *Mol. Pharmacol.* **1999**, *56*, 272.
22. Huang, X.; Suleman, A.; Skibo, E. B. *Bioorg. Chem.* **2000**, *28*, 324.
23. Mosmann, T. *J. Immunol. Methods* **1983**, *65*, 55.
24. Wang, J.; Cieplak, P.; Kollman, P. A. *J. Comput. Chem.* **2000**, *21*, 1049.
25. Edelsbrunner, H.; Facello, M.; Fu, R.; Liang, J. Proceedings of the 28th Hawaii International Conference on Systems Science, 1995.